Hindawi
Adsorption Science & Technology
Volume 2022, Article ID 1922263, 11 pages
https://doi.org/10.1155/2022/1922263

Research Article

Ribociclib-Loaded Ethylcellulose-Based Nanosponges: Formulation, Physicochemical Characterization, and Cytotoxic Potential against Breast Cancer

Mohammed Muqtader Ahmed,[1] **Farhat Fatima**,[1] **Amer Alali**,[1] **Mohd Abul Kalam**,[2,3] **Khalid Alhazzani**,[4] **Saurabh Bhatia**,[5,6] **Sultan Alshehri**,[3] **and Mohammed M. Ghoneim**[7]

[1]*Department of Pharmaceutics, College of Pharmacy, Prince Sattam Bin Abdulaziz University, PO Box 173, Al-Kharj 11942, Saudi Arabia*
[2]*Nanobiotechnology Unit, Department of Pharmaceutics, College of Pharmacy, King Saud University, PO Box 2457, Riyadh 11451, Saudi Arabia*
[3]*Department of Pharmaceutics, College of Pharmacy, King Saud University, Riyadh 11451, Saudi Arabia*
[4]*Department of Pharmacology and Toxicology, College of Pharmacy, King Saud University, PO Box 2457, Riyadh 11451, Saudi Arabia*
[5]*Natural and Medical Sciences Research Center, University of Nizwa, Birkat Al-Mauz, Oman*
[6]*School of Health Science, University of Petroleum and Energy Studies, Dehradun, Uttarakhand, India*
[7]*Department of Pharmacy Practice, College of Pharmacy, AlMareefa University, Al-Diriyah 13713, Saudi Arabia*

Correspondence should be addressed to Mohammed Muqtader Ahmed; mo.ahmed@psau.edu.sa

Received 18 January 2022; Revised 16 February 2022; Accepted 26 February 2022; Published 14 March 2022

Academic Editor: Lakshmipathy R

In the present study, ribociclib-loaded nanosponges (RCNs) composed of ethylcellulose and polyvinyl alcohol were developed using an emulsion-solvent evaporation method. Preliminary evaluations of the developed RCNs (RCN1 to RCN7) were performed in terms of size, polydispersity index (PDI), zeta potential (ZP), entrapment efficiency (EE), and drug loading (DL), which allowed us to select the optimized formulation. RCN3 was selected as the optimized carrier system with particle size (363.5 ± 4.8 nm), PDI (0.292 ± 0.012), zeta potential (−18.5 ± 0.05 mV), EE (81.35 ± 1.64%), and DL (21.96 ± 0.28%). Further, the optimized nanosponges (RCN3) were subjected to FTIR, XRD, DSC, and SEM studies, and results confirmed the proper encapsulation of the drug within the porous polymeric matrix. *In vitro* drug release studies showed that the drug release was significantly enhanced with a maximum drug release through RCN3 formulation (81.85 ± 0.37%) and followed the Higuchi model. Moreover, the RCN3 system showed greater cytotoxicity than free ribociclib (RC) against MDA-MB-231 and MCF-7 breast cancer cell lines. The percentage of apoptosis induced by RCN3 was found significantly higher than that of free RC ($p < 0.05$). Overall, ribociclib-loaded ethylcellulose nanosponges could be a potential nanocarrier to enhance the effectiveness of ribociclib in breast cancer treatment.

1. Introduction

Breast cancer (BC) is considered one of the most common and fatal cancer types detected in women globally [1–4]. It has been believed that BC is the second foremost reason for death after mortalities caused by lung cancer [4–8]. Current developments in explaining the molecular/cellular mechanisms associated with ER+ and TNBC, signaling pathways, and cellular cycle controlling proteins have paved a path for merging endocrinotherapies with the targeted therapeutic agents [9–12]. Moreover, downregulation of cell proliferation is facilitated by unusual stimulation of the cellular cycle mechanism based on the biological effect of cyclin-dependent kinase (CDK) [13]. The development of

nonperceptive CDK inhibitors was found to be futile because of the mutual lack of efficiency and extreme toxicity described through clinical/preclinical trials performed over various cancer types [14]. The clinically established ribociclib (RC), abemaciclib, and palbociclib, classified as second-generation CDK4/6-targeting inhibitors, have showed potential anticancer activities in patients diagnosed with (HER-2) BC [15, 16]. Amongst these inhibitors, RC has been proven as a vastly discerning CDK4/6-selective inhibitor [17], and it acts by specifically merging with the ATP-binding pockets of CDK4/6 [18–21]. Nowadays, numerous preclinical and clinical trials are going on concerning RC administration for the effective mitigation of various tumor types such as non-small-cell lung cancer, BRAFV600 cervical cancers, NRAS-mutant melanomas, neuroblastoma, thyroid cancers, lymphoma, and others [22–24]. In one of the preclinical analyses, it was reported that the RC exhibited potential inhibitory activities principally against the ER+ cell lines, signifying that (ER+) BC might be predominantly liable to CDK4/6 inhibition [25, 26]. It has been noticed that RC as a single moiety or in combination has exhibited potential anticancer activity and also has been found to be efficient to overcome the issues associated with resistance, established through clinical or preclinical studies. For instance, combined dosing of RC with alpelisib (PI3K inhibitor) resulted in improved tumor deterioration, augmented response rates, and development free existence than the single-drug moieties [26, 27]. In another study, the combined treatment of RC and letrozole reduced the cell proliferation more evidently than the single drugs in the treated grade II/III (HR+) BC and (HER2-) BC cell lines [26]. Despite numerous therapeutic activities of RC against BC, its release and targeting behavior at a specific site have been always a major concern, leading to its poor bioavailability. RC is classified as BCS IV drug and demonstrates low solubility and permeability that limits the bioavailability of drug [28]. Its clinical effectiveness is insufficient at the therapeutic level, resulting in an increase in dosage frequency or side effects from high doses. There has not been much work done in the nanocarrier system to address the issue. To overcome these issues, recently it was formulated as polymeric micelles [29] and a nanostructure lipid carrier [30] in order to enhance solubility and bioavailability of RC. Repurposing of RC for the treatment of breast cancer in a nanosponge formulation is a novel approach. For this, RC-loaded ethylcellulose-based nanosponges were developed and evaluated and optimized. Furthermore, anticancer activity of RC and RC-loaded ethylcellulose-based nanosponges was determined in MDA-MB-231 and MCF-7 breast cancer cells by examining cell viability and apoptosis.

2. Materials and Methods

2.1. Materials. Ribociclib (RC) was procured from Mesochem Technology (Beijing, China), and ethylcellulose and polyvinyl alcohol (MW-85,000–124,000) were purchased from Loba Chemie, India. Organic solvent methylene chloride (MC), Dulbecco's Modified Eagle's Medium (DMEM), and Fetal Bovine Serum (FBS) were obtained from Sigma-Aldrich, St. Louis, USA. All other chemical reagents were of analytical grade and were used as received.

2.2. Development of Ribociclib-Loaded Nanosponges. Ethylcellulose-based ribociclib-loaded nanosponges (RCNs) were prepared as per the method reported by Ahmed et al. [31], by using an emulsion-solvent evaporation approach. Accurately weighed ribociclib (50 mg) was dissolved in 5 mL of methylene chloride and vortexed followed by an addition of polymer ethylcellulose (EC) (25-100 mg). Drug-polymer organic solution was then ultrasonicated for 3 minutes in an ultrasonic water bath (Daihan Scientific, Model: WUG-D06H, Gangwon, Korea) to complete the dissolution of added solids. Aqueous stabilizer solution (25-100 mL) was prepared by dissolving PVA in distilled water (0.5% w/v), and the dispersion was mixed with an ultradisperser (IKA T 25 digital Ultra-Turrax®, Staufen, Germany) for 5 minutes. Emulsification was achieved by adding the organic solution (drug-polymer solution) to the aqueous solution in a jacketed ice bath using a sonication probe (435A), programmed for 5 minutes with a 5 sec on-off cycle at 65% amplitude (probe sonicator, Model-FB120, Fisher Scientific, Massachusetts, USA). Nanomaterial colloidal dispersion was placed on the ceramic-coated aluminum-plated magnetic stirrer (MS-20D, Witeg Labortechnik GmbH, Wertheim, Germany) stirred at 1000 rpm to evaporate organic solvent for about 24 h under atmospheric conditions. Colloidal aqueous dispersion was then ultracentrifuged (Eppendorf, model 5418R, Hamburg, Germany) for 2 hours at 8000 rpm. The sediment was then recovered and washed with Milli-Q water ($n = 3$) to remove the adsorbed PVA. Finally, ribociclib-loaded nanosponge slurry was lyophilized and freeze-dried (Millrock Technology, New York, USA). The drug amount was kept constant (50 mg) in all seven nanocarriers. The ratio of EC and PVA was altered to optimize nanosponges (Table 1). The fluffy-spongy matrix-nanosponges were then coded and preserved in a capped glass vial until further characterizations [31].

2.3. Evaluation of Particle Size, Polydispersity Index, and Zeta Potential. Dynamic light scattering (Zetasizer Nano ZS instrument, Malvern Instruments, UK) was used to determine the mean particle diameter and polydispersity index (PDI) of RCNs. Samples under the study were diluted with Milli-Q water (1 : 200) and sonicated for 2 minutes to break particle agglomerates. Diluted particle dispersion was then filled into the cuvette fixed with the copper alloy electrode. The sample holder was then placed into the particle analyzer. The laser beam passed at 900, and parameters were set to analyze particle size and potential [32]. All the measurements were taken in triplicate ($n = 3$). The ZP values of each nanosponge were measured (Zetasizer Nano ZS instrument, Malvern Instruments, UK). The same method was adopted for ZP measurement except diluted samples were transferred into a glass electrode [33].

2.4. Percent Drug Entrapment and Loading Estimation. Entrapment efficiency (EE) and drug loading (DL) in the developed nanosponges for each formula were estimated by an indirect method [34]. The freshly prepared nanosponge solution was centrifuged (Hermle Labortechnik, Z216MK, Wehingen, Germany) at 12,000 rpm for 10

Table 1: Composition of ribociclib-loaded nanosponges.

Nanosponges	Ribociclib (mg)	Ethylcellulose (mg)	PVA 0.5%, *w*/*w* (mL)
RCN1	50	25	25
RCN3	50	25	50
RCN3	50	50	25
RCN4	50	50	50
RCN5	50	25	100
RCN6	50	50	100
RCN7	50	100	100

minutes. After centrifugation, the supernatant of each sample was collected in the microcentrifuge tube and analyzed using an ultraviolet-spectrophotometer (Jasco UV/Visible Spectrophotometer V-630 Japan) at λ max = 275 nm [35]. The %EE and %DL were calculated using equations:

$$\begin{aligned} \text{EE}\,(\%) &= \frac{T_d - S_d}{T_D} \times 100, \\ \text{DL}\,(\%) &= \frac{\text{Total entrapped drug}}{\text{Weight of nanosponges}} \times 100, \end{aligned} \tag{1}$$

where T_d is the theoretical drug content, S_d is the amount of free drug in the supernatant, and T_D is the theoretically calculated total drug amount.

2.5. FTIR Spectroscopy. The possibilities of any chemical interaction between drug and excipients are detected by FTIR analysis. KBr pellets were prepared for pure drug RC and optimized nanosponge (RCN3), separately. First collect an interferogram of a KBr signal (100% transmittance) using an interferometer, to validate the instrument; then, RC and optimized RCN were analyzed in the wavelength range of 4000-400 cm^{-1} using the FTIR spectrophotometer (Jasco 4600 Mid-IR FTIR Spectrometer, Japan) [36–38].

2.6. Differential Scanning Calorimetry. Thermal analysis of drug (RC) and nanosponges (RCN3) was performed by DSC study, wherein the sample (5 mg) under study was crimped in an aluminum pan and then analyzed against an empty reference pan. The thermal properties of pure RC and optimized RCN were analyzed within a temperature range of 30–250°C at a heating rate of 10°C/min using the DSC instrument (DSC N-650, Scinco, Seoul, Korea).

2.7. X-Ray Diffraction (XRD) Analysis. X-ray diffraction (XRD) study is one of the most prominent techniques for the characterization of NSs [38]. XRD studies are performed to estimate the physical property of the samples, whether the compound exhibits crystalline or amorphous state. The physical nature of the pure RC and optimized RCN3 was evaluated at 2θ angle in the range of 5-60° using an X-ray diffractometer (Altima IV Regaco, Tokyo, Japan).

2.8. Morphology by Scanning Electron Microscopy (SEM). The morphology of the optimized nanosponge (RCN3) was examined using SEM (JEOL JSM-5900-LV, Tokyo, Japan) operated at 15 kV. Freeze-dried powder of RCN3 was coated with a thin layer of gold under vacuum.

2.9. In Vitro Drug Release Studies. The nature of drug release and kinetic is assessed through *in vitro* drug release studies in biorelevant physiological medium. Based on these studies, the mechanism of drug release was also examined. The study was performed by using a dialysis bag method [38]. Briefly, 10 mL of both pure RC suspension and optimized nanosponge (RCN3) containing 10 mg equivalent of amount of drug was added in the respective dialysis bags (cut-off mol. weight 12,000 Daltons) followed by dipping of these bags into a beaker comprising 100 mL of phosphate buffer solution (PBS) pH 7.4 maintained at 37 ± 2°C and was kept over a magnetic stirrer at 100 rpm. At predetermined time intervals, 1 mL of sample aliquots was withdrawn from respective dialysis bags and was simultaneously replaced with freshly prepared PBS. Finally, the withdrawn aliquots of respective samples were measured at wavelength 275 nm [36] using UV/Vis spectroscopy (Jasco UV spectrophotometer V-630, Japan). All the specimens for each sample were executed in triplicate ($n = 3$). Moreover, the kinetics and mechanism behind the drug release from RCN3 were assessed through fitting the results of cumulative drug release studies into various kinetic mathematical modelling, such as zero-order, first-order, Higuchi, and Korsmeyer-Peppas models, and were calculated via the following equations:

$$\begin{aligned} \text{Zero order, } Qt &= Q0 + k0t, \\ \text{First order, } \log Qt &= \frac{\log Q0 - k1t}{2.303}, \\ \text{Higuchi, } Qt &= \frac{kHt1}{2}, \\ \text{Korsmeyer-Peppas, } \frac{Mt}{M\infty} &= ktn, \end{aligned} \tag{2}$$

where Qt is the total drug dissolved in time t, $Q0$ is the total drug dissolved in the dispersion medium at the initial stage, $k0$ is the zero-order kinetic constant, $k1$ is the first-order rate constant, and $kHt1/2$ is the Higuchi model constant. Mt and $M\infty$ are cumulative drug release at time t and infinite time, respectively; k is the rate constant of RCNs; t is the release time; and n is the diffusion exponent representing the release mechanism.

2.10. MTT Assay against Breast Cancer Cell Lines. The cell viability assay was performed to assess the anticancer efficacy of pure RC and RCN3 against selective human breast cancer cell lines (MCF-7 and MDA-MB-231). Human breast cancer cell lines MCF-7 (ATCCC®RL-3435™) and MDA-MB-231 (ATCCC®HTB-26™) were obtained from the American Type Culture Collection (ATCC, Manassas, VA, USA). The *in vitro* cell viability study was accomplished through the 2,5-diphenyl-2H-tetrazolium bromide (MTT) assay using a colorimetric method. Before analysis, both the cell lines were passaged in DMEM culture medium supplemented with FBS (10%) and were then incubated in an incubator overnight maintained at 37°C under CO_2

Table 2: Evaluation of ribociclib-loaded nanosponges (RCN1-RCN7).

Nanosponges	Size ± SD (nm)	PDI	ZP ± SD (mV)	%EE	%DL
RCN1	585.2 ± 2.2	0.643 ± 0.005	−12.92 ± 0.04	49.26 ± 1.13	12.70 ± 0.51
RCN2	466.9 ± 2.3	0.320 ± 0.009	−15.98 ± 0.08	61.95 ± 1.08	13.96 ± 0.14
RCN3	363.5 ± 4.8	0.292 ± 0.012	−18.5 ± 0.05	81.35 ± 1.64	21.96 ± 0.28
RCN4	440.6 ± 2.2	0.514 ± 0.004	−9.49 ± 0.01	36.04 ± 0.91	10.97 ± 0.35
RCN5	734.9 ± 3.1	0.726 ± 0.006	−6.49 ± 0.02	23.28 ± 0.84	8.52 ± 0.15
RCN6	546.8 ± 4.6	0.272 ± 0.007	−14.9 ± 0.04	69.68 ± 1.11	17.46 ± 0.23
RCN7	610.4 ± 8.3	0.392 ± 0.014	−11.93 ± 0.06	45.21 ± 1.46	11.21 ± 0.17

PDI: polydispersity index; ZP zeta potential; EE entrapment efficiency; DL drug loading.

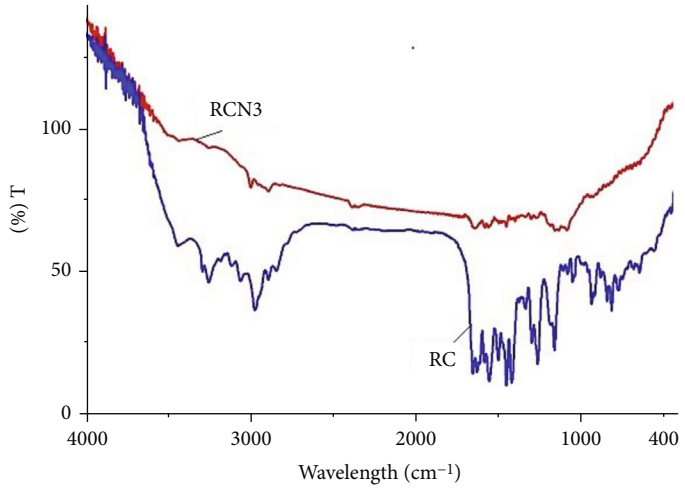

Figure 1: Comparative FTIR spectra of pure RC and optimized nanosponge (RCN3).

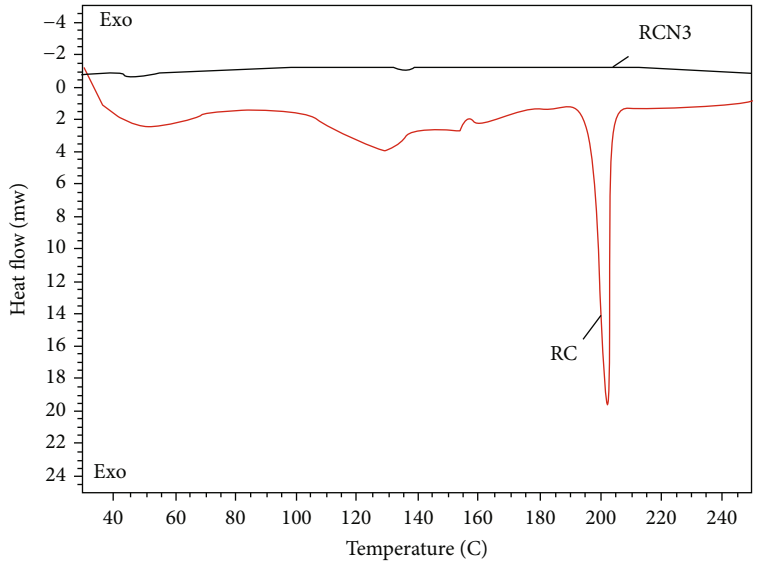

Figure 2: Comparative DSC spectra of pure RC and optimized nanosponge (RCN3).

environment. Later, 1000 μL of these cell suspensions (~5×10^4 cells/mL) was loaded into a sterilized 24-well plate and was kept in the incubator undisturbed overnight maintained at 37°C. After incubation, each of the samples was added distinctly into pretreated (transferred from a 24-well plate) 96-well plates. Further, 100 μL of the earlier prepared MTT solution (5% w/v) was treated to the separate wells and were incubated for 3 hours at 37°C. Finally, optical density of

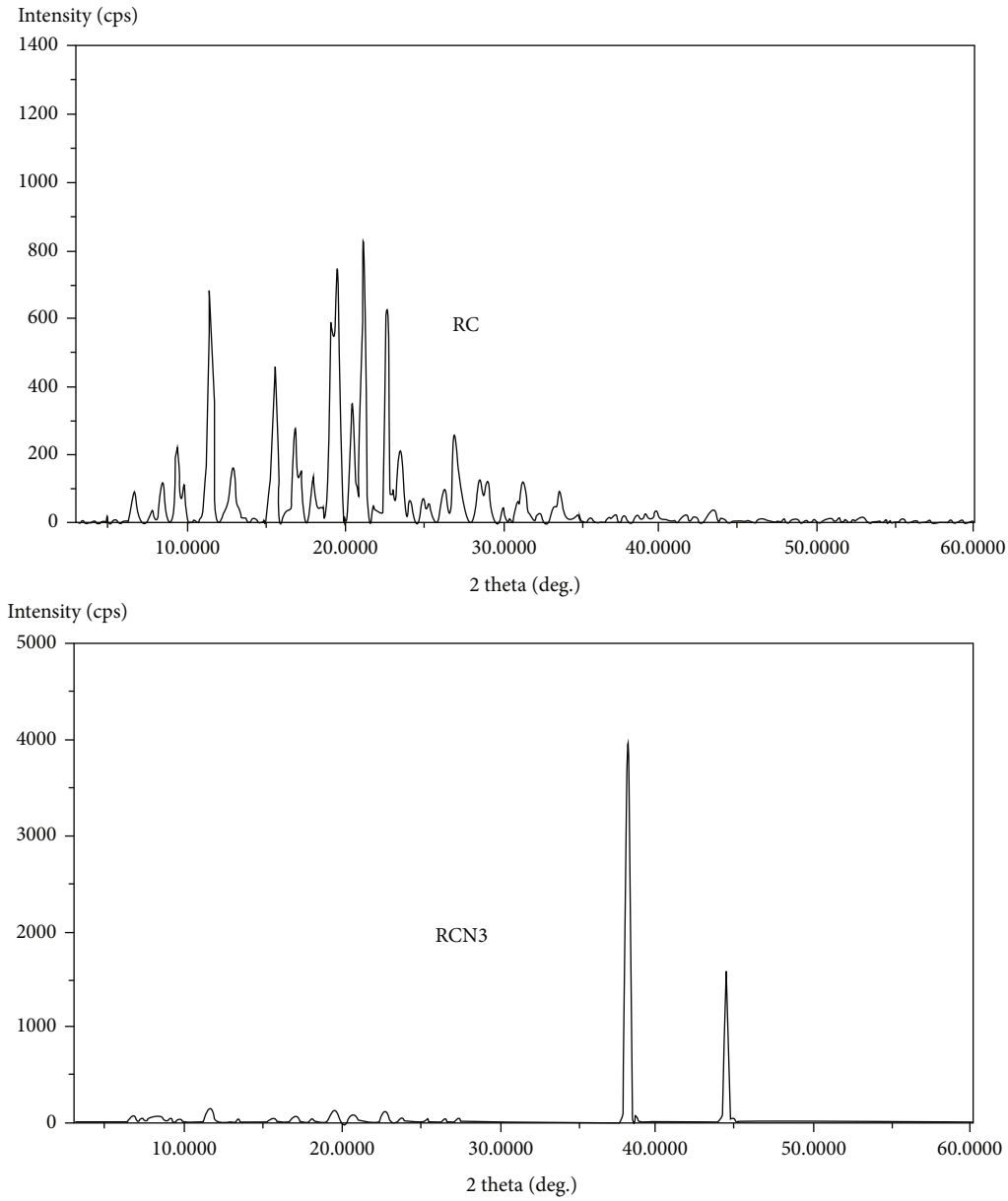

Figure 3: Comparative XRD pattern of pure RC and optimized nanosponge (RCN3).

each sample was estimated at 490 nm with the help of the ELISA microplate reader (Thermo Fisher Scientific, USA) to determine the percent cell viability; also, IC50 was measured.

$$\text{Cell Viability (\%)} = \frac{\text{Mean absorbance of sample}}{\text{Mean absorbance of control}} \times 100. \quad (3)$$

2.11. Apoptosis Studies by the Annexin V-Propidium Iodide Method. Apoptosis induced by control, pure RC, and optimized nanosponge (RCN3) was studied by the Annexin V staining technique. The 1×10^3 cells/well were seeded in six-well plates and incubated with IC50 concentration of optimized formulation (RCN3) for 24 h at 37°C, collected, and centrifuged for 5 min. The cells were then washed twice in PBS and resuspended at room temperature. The mixture was incubated for 5 minutes at 25°C with Annexin V-FITC (10 μL) and propidium iodide (PI) solution (5 μL). A flow cytometer was used to do the study.

2.12. Statistical Analysis. Results were expressed as the mean ± standard error of the mean (SEM). Statistical variations of different treatment groups were analyzed according to one-way analysis of variance (ANOVA) followed by post hoc Tukey's test. $p < 0.05$ was considered statistically significant. Statistical analysis was performed using the GraphPad Prism program (version 4) (GraphPad Software, San Diego, CA, USA).

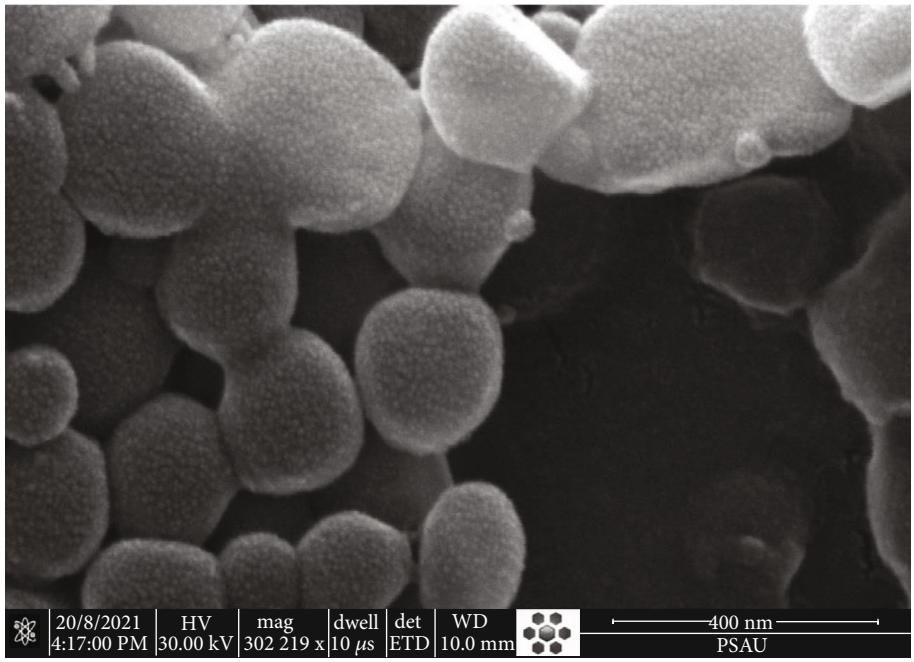

Figure 4: SEM images of the optimized nanosponge (RCN3).

3. Results and Discussion

3.1. Particle Size, PDI, ZP, %EE, and %DL. The particle size analysis of the developed RC-loaded polymeric nanosponges was assessed through DLS studies. The particle size, PDI, and ZP of the nanosponges (RCN1-RCN7) were measured in the range of 363.5 ± 4.8-734.9 ± 3.1 nm, 0.292 ± 0.012-0.726 ± 0.006, and -6.49 ± 0.02 to -18.5 ± 0.05 mV, respectively (Table 2). Based on the results of particle size analysis, RCN3 was selected as the optimized formulation with optimized particle size, PDI, and ZP values of 363.5 ± 4.8 nm, 0.292 ± 0.012, and -18.5 ± 0.05 mV, respectively. From the results of zeta potential, it was suggested that the negative surface charge of the formulations was probably due to ethylcellulose, which further assisted in particle-particle repulsion [38, 39]. It is believed that the values of $\zeta P \geq \pm 30$ mV indicate the formation of a stable dispersion; however, it has to be mentioned that the usual Smoluchowski method to calculate ζP is only valid for hard spheres. In this case, due to the soft nature of NSs, ζP calculated by conventional analysis does not reflect the state of agglomeration or stability. Our soft NS particles were stable despite $\zeta P < \pm 30$ mV [40]. Furthermore, the results of %EE and %DL of the nanosponges (RCN1-RCN7) were demonstrated in Table 2. The %EE and %DL were found to be in the range of 23.28%-81.35% and 8.52%-21.96%, respectively. RCN3 exhibited the most suitable outcomes of %EE (81.35 ± 1.64) and %DL (21.96 ± 0.078).

3.2. FTIR Spectroscopy. FTIR spectra of pure drug RC and RCN3 are presented in Figure 1. Typical peaks of pure RC were assigned at 3200 cm^{-1} for NH stretching, 2914 cm^{-1} for C=H stretching, 1631 cm^{-1} for C=O stretching, and 1529 cm^{-1} for NH bending vibration. Results showed that the spectrum of RCN3 exhibited shifting/disappearance of identical peaks of RC with the reduction in intensity in the fingerprint region of the drug. This indicates that the drug was physically entrapped within the polymer matrix [41].

3.3. Differential Scanning Calorimetry. As shown in the results of DSC analysis in Figure 2, it was observed that the sharp endothermic peak of pure RC at 201.12°C [42] completely disappeared in the case of RCN3. This is possibly due to the proper entrapment of the drug within the polymer-ethylcellulose.

3.4. X-Ray Diffraction (XRD) Analysis. XRD spectra of pure drug RC and optimized nanosponge (RCN3) are presented in Figure 3. XRD diffractogram of RC exhibited various characteristic sharp and intense peaks at degree 2-theta 6.7°, 8.5°, 9.4°, 9.8°, 11.5°, 12.9°, 15.6°, 16.9°, 18.0°, 19.2°, 19.6°, 21.2°, and 22.7° as reported in literature [42]. However, various drug peaks disappeared or were reduced in intensity except two sharp peaks at 38.1° and 44.3° which could be seen in RCN3, probably due to the presence of the polymer. Thus, it clearly indicated that the RC was adequately encapsulated within the polymer matrix in the nanosponge. The disappearance/reduction in peak intensity is due to transformation of crystalline drug into amorphous form [42].

3.5. Morphology by Scanning Electron Microscopy (SEM). The morphology of the optimized RC-loaded nanosponge (RCN3) is presented in Figure 4. Particles could be seen in nanosize range with a spongy porous surface. The particles were connected to each other and form a bridge, probably

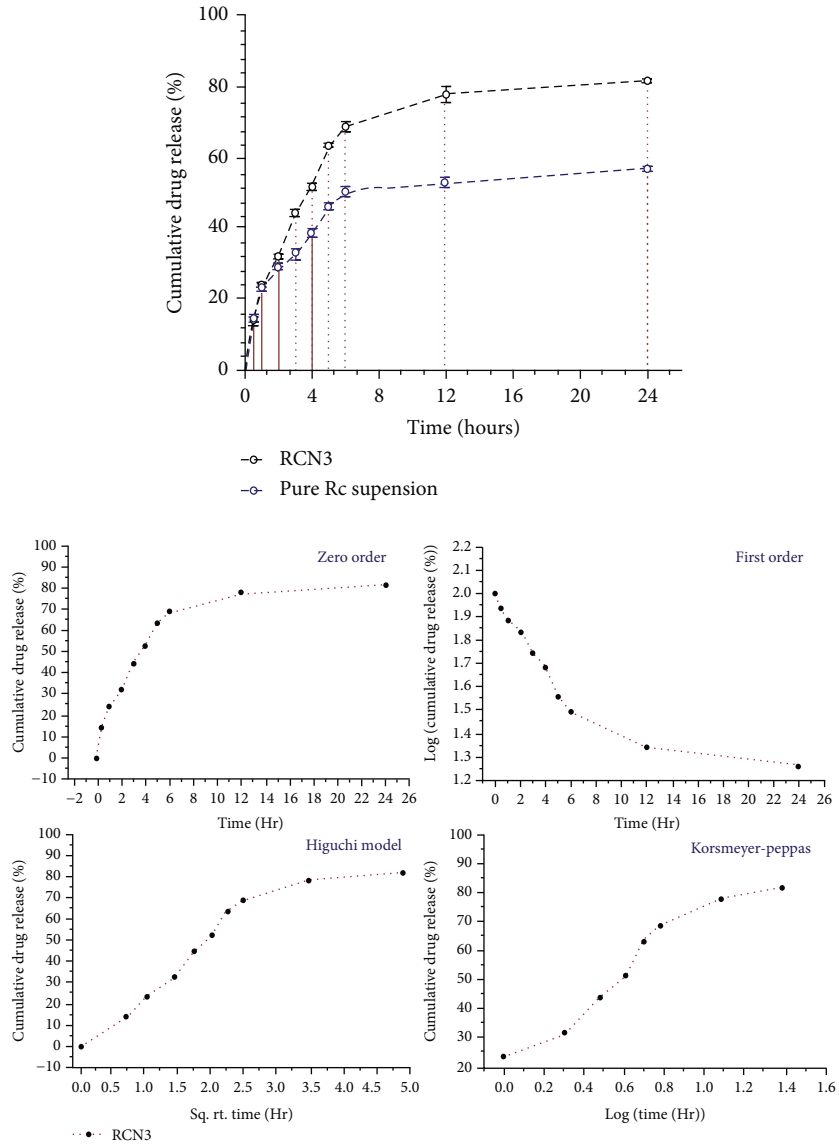

Figure 5: Drug release profile and kinetic model of RCN3.

due to the presence of PVA remnants on the surface of the nanosponge. The size of particles observed by SEM was approximately identical to that observed by the DLS method.

3.6. In Vitro Drug Release Studies. *In vitro* drug release study was performed using a dialysis bag method, and release data of drug from the nanomaterials assist in assessing the safety and efficacy. Drug release profiles for both pure RC suspension and optimized formulation (RCN3) have been represented in Figure 5. Results showed that the drug release was sustained in RCN3 in comparison to pure drug suspension. An initial burst drug release was observed within the first 5 h, followed by sustained release till 24 h. Burst release effect could be due to the adsorption or distribution of RC on the nanosponge surface that permits instant drug dissolution on contact wetting with diffusion medium [39]. The release pattern with an initial burst effect followed by a sustained release by the fraction of drug located inside the porous matrix represents the biphasic drug release profile [43]. The cumulative drug release values for both pure RC suspension and RCN3 were found to be 81.85% ± 0.37 and 57.02% ± 0.56, respectively. From the results, it was estimated that the polymer played a crucial role in increasing the sustained release properties of the drug, probably because of slower dispersion of aqueous medium inside the porous matrix. Almutairy et al. discussed that the release of olmesartan from the ethylcellulose nanosponges was in a sustained pattern, which could be due to viscous and swelling nature of the polymer used EC [39].

Additionally, the results of release kinetic of the drug from optimized nanosponges are shown in Figure 5. The values for regression coefficient (r^2) were found to be different, i.e., for zero-order ($r^2 = 0.8298$), first-order ($r^2 = 0.7745$), and Higuchi models ($r^2 = 0.9441$). From the results, it was

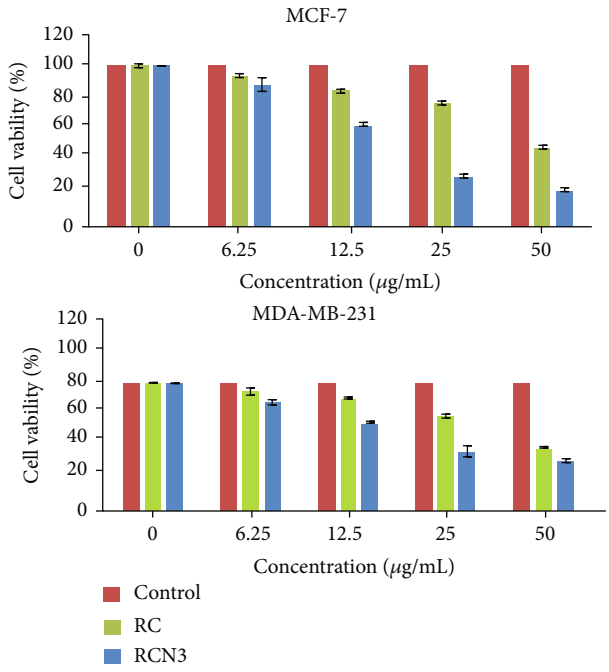

Figure 6: Percent cell viability of pure RC and optimized nanosponge (RCN3) against MDA-MB-231 and MCF-7 breast cancer cell lines.

considered that the Higuchi model acted as a best-fit model, signifying sustained drug release from the porous nanomatrix [44]. Figure 5 shows the Higuchi release kinetic graph plotted from cumulative (%) drug release against the square root of time in hours. Sustained drug release from the ethylcellulose for a prolonged time period could be due to the fact that the drug release was diffusion controlled through the porous nanocarrier [35]. Sustained release of RC from nanosponges could be beneficial for the treatment of breast cancer.

3.7. MTT Assay against Breast Cancer Cell Lines. The encapsulation of pure RC within the polymeric matrix significantly enhanced its targetability, leading to improved anticancer effects against both the breast cancer cell lines. Gadag et.al reported that RC is a potential cyclin-dependent kinase (CDK) inhibitor and could be effectively used for the breast cancer [45]. The MTT assay exhibited concentration-dependent reduction in percent cell viability for pure drug RC and the optimized nanosponge RCN3 against MCF-7 and MDA-BD-231 breast cancer cell lines (Figure 6). The RCN3 exhibited significant reduction in cell viability (87.9, 63.0, 30.8, and 22.3% at 6.25, 12.25, 25, and 50 μg/mL) in comparison to pure drug RC (93.8, 84.0, 76.8, and 49.1% at 6.25, 12.25, 25, and 50 μg/mL), against MCF-7 cell lines, respectively, and the cell viability against MDA-DB-231 cell lines showed 84.4, 68.8, 46.0, and 39.4% at 6.25, 12.25, 25, and 50 μg/mL) in comparison to pure drug RC (93.1, 87.8, 73.9, and 48.8% at 6.25, 12.25, 25, and 50 μg/mL), against MCF-7 cell lines, respectively. The IC50 values were calculated for the RC and RCN3 as $48.66 \pm 0.5\,\mu$g/mL and $17.39 \pm 0.46\,\mu$g/mL in MCF-7 cell lines and $49.51 \pm 0.76\,\mu$g/mL and $23.09 \pm 2.11\,\mu$g/mL in MDA-MB-231 cell lines, respectively. The anticancer effect of RCN3 was enhanced to 2.14-fold and 2.79-fold in comparison to free drug (RC) against MDA-MB-231 and MCF-7 breast cancer lines, respectively. The different sensitivity of ribociclib-loaded nanosponges to MCF-7 and MDA-MB-231 cells may be due to the differences in the expression of breast cancer-related proteins. MCF-7 is a glucocorticoid receptor (estrogen and progesterone) epithelial luminal-positive breast cancer cell [46]. It is a widely studied model for hormone-dependent human breast cancer. MDA-MB-231 is a triple-negative breast cancer cell (lack of estrogen and progesterone). The MDA-MB-231 cell line used as a model for human breast cancer cells exhibits an estrogen-independent state and does not express an estrogen receptor. The lack of estrogen and progesterone in MDA-MB-231 is the key for the different sensitivity between MCF-7 and MDA-MB-231 [46]. The different sensitivity of these two cell lines MCF-7 and MDA-MB-231 depends on the chemotherapeutics. Anticancer data exhibited that the ribociclib, when entrapped in nanosponges, showed potential cytotoxicity at lower concentrations than free drug ribociclib. In general, a high dose with multiple regimens is needed to get the chemotherapeutic effects leading to severe or multiple adverse effects due to cell toxicity of anticancer drugs. Henceforth, the dose and frequency of drug administration could be reduced by the developed RCN3 nanosponges with sustained drug release.

3.8. Apoptosis Studies by the Annexin V-Propidium Iodide Method. Apoptosis studies were performed by flow cytometry to explore the apoptotic potential of RCN3 against MCF-7 cell lines. The results show an excellent apoptotic activity of parent drug RC in comparison to control (Figure 7). However, optimized RCN3 shows a sharp rise in cell death in the late apoptosis phase in comparison to both control and pure drug RC-treated MCF-7 cells. A remarkable decrease in narcosis (N) was observed with RC and RCN3

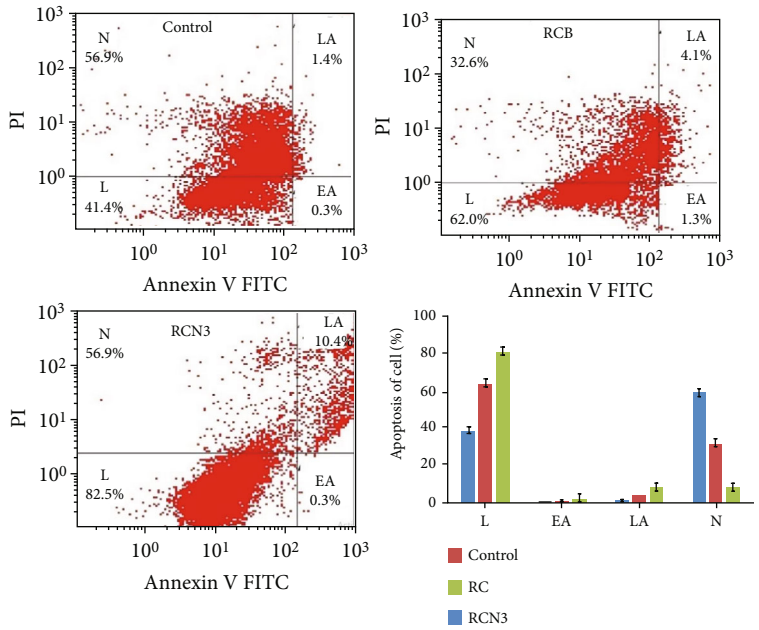

Figure 7: Apoptosis activity of control, free RC, and RCN3 against MCF-7 breast cell lines. Bar graph showing percent of live cells (L), early apoptosis (EA), late apoptosis (LA), and narcosis (N) induced by different treatments under investigation. Data are expressed as mean ± SD ($n = 3$). ∗ indicates significant difference between RCN3 ($p \leq 0.05$) and free RC and control.

treatment compared to control. Furthermore, the percentage of early apoptosis (EA) and late apoptosis (LA) with RCN3 (10.4%) was significantly higher ($p \leq 0.05$) in comparison to free RC (4.1%) and control (1.4%). Therefore, the nanosponge of RC confirmed antitumor activity against MCF-7 breast cell lines. It was revealed from apoptosis that the RCN3 nanosponge was more cytotoxic than free RC to kill breast cancerous cells.

4. Conclusion

We successfully developed and evaluated ribociclib-loaded ethylcellulose-based nanosponges as a potential treatment for breast cancer. The prepared nanosponges were optimized based on particle size, PDI, zeta potential, entrapment efficiency, and drug loading. The optimized nanosponges improved the release properties of the ribociclib and also showed higher cytotoxic and apoptotic cell death in MDA-MB-231 and MCF-7 cell lines. Based on overall findings, repurposing ribociclib by encapsulation in a nanosponge could be an effective approach for breast cancer treatment.

Data Availability

The data presented in this study are available on request from the corresponding author.

Conflicts of Interest

The authors declare that they have no conflicts of interest.

Authors' Contributions

M.M.A. and F.F. were responsible for the conceptualization. F.F. and M.A.K. were responsible for the methodology. K.A. was responsible for the investigation. A.A. was responsible for the resources. K.A. was responsible for the data curation. M.M.A. was responsible for the original draft preparation. A.Z. and S.B. reviewed and edited the paper. M.M.A. was responsible for the supervision. M.M.A. was responsible for the project administration. M.M.A. was responsible for the funding acquisition. All authors have read and agreed to the published version of the manuscript.

Acknowledgments

The authors extend their appreciation to the Deputyship for Research & Innovation, Ministry of Education, in Saudi Arabia for funding this research work through the project number IF/PSAU-2021/03/18862.

References

[1] C. DeSantis, J. Ma, L. Bryan, and A. Jemal, "Breast cancer statistics, 2013," *CA: a Cancer Journal for Clinicians*, vol. 64, no. 1, pp. 52–62, 2014.

[2] L. A. Torre, F. Islami, R. L. Siegel, E. M. Ward, and A. Jemal, "Global cancer in women: burden and trends," *Cancer Epidemiology, Biomarkers & Prevention*, vol. 26, no. 4, pp. 444–457, 2017.

[3] M. Brown, A. Tsodikov, K. R. Bauer, C. A. Parise, and V. Caggiano, "The role of human epidermal growth factor receptor 2 in the survival of women with estrogen and progesterone receptor-negative, invasive breast cancer: the California

Cancer Registry, 1999-2004," *Cancer*, vol. 112, no. 4, pp. 737–747, 2008.

[4] R. Dent, M. Trudeau, K. I. Pritchard et al., "Triple-negative breast cancer: clinical features and patterns of recurrence," *Clinical Cancer Research*, vol. 13, no. 15, pp. 4429–4434, 2007.

[5] G. Gu, D. Dustin, and S. A. Fuqua, "Targeted therapy for breast cancer and molecular mechanisms of resistance to treatment," *Current Opinion in Pharmacology*, vol. 31, pp. 97–103, 2016.

[6] A. Lee and M. B. A. Djamgoz, "Triple negative breast cancer: emerging therapeutic modalities and novel combination therapies," *Cancer Treatment Reviews*, vol. 62, pp. 110–122, 2018.

[7] G. Agarwal, G. Nanda, P. Lal et al., "Outcomes of triple-negative breast cancers (TNBC) compared with non-TNBC: does the survival vary for all stages?," *World Journal of Surgery*, vol. 40, no. 6, pp. 1362–1372, 2016.

[8] G. N. Hortobagyi, S. M. Stemmer, H. A. Burris et al., "Ribociclib as first-line therapy for HR-positive, advanced breast cancer," *New England Journal of Medicine*, vol. 375, no. 18, pp. 1738–1748, 2016.

[9] A. Nardone, C. De Angelis, M. V. Trivedi, C. K. Osborne, and R. Schiff, "The changing role of ER in endocrine resistance," *Breast*, vol. 24, pp. S60–S66, 2015.

[10] B. Weigelt, J. L. Peterse, and L. J. van't Veer, "Breast cancer metastasis: markers and models," *Nature Reviews. Cancer*, vol. 5, no. 8, pp. 591–602, 2005.

[11] H. P. Sinn and H. A. Kreipe, "Brief overview of the WHO classification of breast tumors, 4th edition, focusing on issues and updates from the 3rd edition.," *Breast Care*, vol. 8, pp. 149–154, 2013.

[12] C. Michaloglou, C. Crafter, R. Siersbaek et al., "Combined inhibition of mTOR and CDK4/6 is required for optimal blockade of E2F function and long-term growth inhibition in estrogen receptor-positive breast cancer," *Molecular Cancer Therapeutics*, vol. 17, no. 5, pp. 908–920, 2018.

[13] M. Bonelli, S. La Monica, C. Fumarola, and R. Alfieri, "Multiple effects of CDK4/6 inhibition in cancer: from cell cycle arrest to immunomodulation," *Biochemical Pharmacology*, vol. 170, article 113676, 2019.

[14] S. R. Whittaker, A. Mallinger, P. Workman, and P. A. Clarke, "Inhibitors of cyclin-dependent kinases as cancer therapeutics," *Pharmacology & Therapeutics*, vol. 173, pp. 83–105, 2017.

[15] X. Chen, D. Xu, X. Li et al., "Latest overview of the cyclin-dependent kinases 4/6 inhibitors in breast cancer: the past, the present and the future," *Journal of Cancer*, vol. 10, no. 26, pp. 6608–6617, 2019.

[16] T. K. Eggersmann, T. Degenhardt, O. Gluz, R. Wuerstlein, and N. Harbeck, "CDK4/6 inhibitors expand the therapeutic options in breast cancer: palbociclib, ribociclib and abemaciclib," *BioDrugs*, vol. 33, no. 2, pp. 125–135, 2019.

[17] M. Poratti and G. Marzaro, "Third-generation CDK inhibitors: a review on the synthesis and binding modes of palbociclib, ribociclib and abemaciclib," *European Journal of Medicinal Chemistry*, vol. 172, pp. 143–153, 2019.

[18] H. Fang, D. Huang, F. Yang, and X. Guan, "Potential biomarkers of CDK4/6 inhibitors in hormone receptor-positive advanced breast cancer," *Breast Cancer Research and Treatment*, vol. 168, no. 2, pp. 287–297, 2018.

[19] Y. Niu, J. Xu, and T. Sun, "Cyclin-dependent kinases 4/6 inhibitors in breast cancer: current status, resistance, and combination strategies," *Journal of Cancer*, vol. 10, no. 22, pp. 5504–5517, 2019.

[20] A. J. Walker, S. Wedam, L. Amiri-Kordestani et al., "FDA approval of palbociclib in combination with fulvestrant for the treatment of hormone receptor-positive, HER2-negative metastatic breast cancer," *Clinical Cancer Research*, vol. 22, no. 20, pp. 4968–4972, 2016.

[21] D. Kwapisz, "Cyclin-dependent kinase 4/6 inhibitors in breast cancer: palbociclib, ribociclib, and abemaciclib," *Breast Cancer Research and Treatment*, vol. 166, no. 1, pp. 41–54, 2017.

[22] B. Geoerger, F. Bourdeaut, S. G. DuBois et al., "A phase I study of the CDK4/6 inhibitor ribociclib (LEE011) in pediatric patients with malignant rhabdoid tumors, neuroblastoma, and other solid tumors," *Clinical Cancer Research*, vol. 23, no. 10, pp. 2433–2441, 2017.

[23] J. R. Infante, P. A. Cassier, J. F. Gerecitano et al., "A phase I study of the cyclin-dependent kinase 4/6 inhibitor ribociclib (LEE011) in patients with advanced solid tumors and lymphomas," *Clinical Cancer Research*, vol. 22, no. 23, pp. 5696–5705, 2016.

[24] A. C. Wood, K. Krytska, H. T. Ryles et al., "Dual ALK and CDK4/6 inhibition demonstrates synergy against neuroblastoma," *Clinical Cancer Research*, vol. 23, no. 11, pp. 2856–2868, 2017.

[25] G. N. Hortobagyi, "Ribociclib for the first-line treatment of advanced hormone receptor-positive breast cancer: a review of subgroup analyses from the MONALEESA-2 trial," *Breast Cancer Research*, vol. 20, no. 1, pp. 1–11, 2018.

[26] D. Tripathy, A. Bardia, and W. R. Sellers, "Ribociclib (LEE011): mechanism of action and clinical impact of this selective cyclin-dependent kinase 4/6 inhibitor in various solid tumors," *Clinical Cancer Research*, vol. 23, no. 13, pp. 3251–3262, 2017.

[27] M. A. Aboudzadeh, *Emulsion-Based Encapsulation of Antioxidants*, Springer Nature, Cham, Switzerland, 2020.

[28] J. Lai, Y. Tseng, M. Chen, C. F. Huang, and P. M. Chang, "Clinical perspective of FDA approved drugs with P-glycoprotein inhibition activities for potential cancer therapeutics," *Frontiers in Oncology*, vol. 10, 2020.

[29] Z. Fei and M. Yoosefian, "Design and development of polymeric micelles as nanocarriers for anti-cancer ribociclib drug," *Journal of Molecular Liquids*, vol. 329, p. 115574, 2021.

[30] A. Sartaj, L. Biswas, A. K. Verma, P. K. Sahoo, S. Baboota, and J. Ali, "Ribociclib nanostructured lipid carrier aimed for breast cancer: formulation optimization, attenuating *in vitro* specification, and *in vivo* scrutinization," *BioMed Research International*, vol. 2022, Article ID 6009309, 24 pages, 2022.

[31] M. M. Ahmed, F. Fatima, M. K. Anwer, M. J. Ansari, S. S. Das, and S. M. Alshahrani, "Development and characterization of ethyl cellulose nanosponges for sustained release of brigatinib for the treatment of non-small cell lung cancer," *Journal of Polymer Engineering*, vol. 40, no. 10, pp. 823–832, 2020.

[32] M. K. Anwer, M. M. Ahmed, E. Ezzeldin, F. Fatima, A. Alalaiwe, and M. Iqbal, "Preparation of sustained release apremilast-loaded PLGA nanoparticles: *in vitro* characterization and in vivo pharmacokinetic study in rats," *International Journal of Nanomedicine*, vol. 14, pp. 1587–1595, 2019.

[33] M. M. Ahmed, M. S. Alnafisah, M. K. Anwer et al., "Chitosan surface modified PLGA nanoparticles loaded with brigatinib for the treatment of non-small cell lung cancer," *Journal of Polymer Engineering*, vol. 39, no. 10, pp. 909–916, 2019.

[34] M. K. Anwer, M. Mohammad, M. Iqbal et al., "Sustained release and enhanced oral bioavailability of rivaroxaban by PLGA nanoparticles with no food effect," *Journal of Thrombosis and Thrombolysis*, vol. 49, no. 3, pp. 404–412, 2020.

[35] D. R. Paul, "Elaborations on the Higuchi model for drug delivery," *International Journal of Pharmaceutics*, vol. 418, no. 1, pp. 13–17, 2011.

[36] M. M. Ahmed, F. Fatima, M. K. Anwer et al., "Development and characterization of brigatinib loaded solid lipid nanoparticles: in-vitro cytotoxicity against human carcinoma A549 lung cell lines," *Chemistry and Physics of Lipids*, vol. 233, p. 105003, 2020.

[37] F. Fatima, M. F. Aldawsari, M. M. Ahmed et al., "Green synthesized silver nanoparticles using Tridax procumbens for topical application: excision wound model and histopathological studies," *Pharmaceutics*, vol. 13, no. 11, p. 1754, 2021.

[38] M. M. Ahmed, F. Fatima, M. A. Kalam et al., "Development of spray-dried amorphous solid dispersions of tadalafil using glycyrrhizin for enhanced dissolution and aphrodisiac activity in male rats," *Saudi Pharmaceutical Journal*, vol. 28, no. 12, pp. 1817–1826, 2020.

[39] B. K. Almutairy, A. Alshetaili, A. S. Alali, M. M. Ahmed, M. K. Anwer, and M. A. Aboudzadeh, "Design of olmesartan medoxomil-loaded nanosponges for hypertension and lung cancer treatments," *Polymers*, vol. 13, no. 14, p. 2272, 2021.

[40] D. Lerche and T. Sobisch, "Evaluation of particle interactions by in situ visualization of separation behaviour," *Colloids and Surfaces A: Physicochemical and Engineering Aspects*, vol. 440, pp. 122–130, 2014.

[41] M. K. Anwer, M. A. Al-Mansoor, S. Jamil, R. Al-Shdefat, M. N. Ansari, and F. Shakeel, "Development and evaluation of PLGA polymer based nanoparticles of quercetin," *International Journal of Biological Macromolecules*, vol. 92, pp. 213–219, 2016.

[42] A. Wolfgang and L. Frank, *Crystalline forms of ribociclib free base. European Patent No. EP 3 156 406 A1*, European Patent Application, 2016.

[43] M. Lingam, T. Ashok, V. Venkateswarlu, and R. Y. Madhusudan, "Design and evaluation of a novel matrix type multiple units as biphasic gastroretentive drug delivery systems," *AAPS PharmSciTech*, vol. 9, no. 4, pp. 1253–1261, 2008.

[44] M. K. Anwer, E. A. Ali, M. Iqbal et al., "Development of sustained release baricitinib loaded lipid-polymer hybrid nanoparticles with improved oral bioavailability," *Molecules*, vol. 27, no. 1, p. 168, 2022.

[45] S. Gadag, S. Sinha, Y. Nayak, S. Garg, and U. Y. Nayak, "Combination therapy and nanoparticulate systems: smart approaches for the effective treatment of breast cancer," *Pharmaceutics*, vol. 12, no. 6, p. 524, 2020.

[46] T. Jia, L. Zhang, Y. Duan et al., "The differential susceptibilities of MCF-7 and MDA-MB-231 cells to the cytotoxic effects of curcumin are associated with the PI3K/Akt-SKP2-Cip/Kips pathway," *Cancer Cell International*, vol. 14, no. 1, p. 126, 2014.